Fluorescence Decay Kinetics and Structure of Aggregated Tetrakis(*p*-Sulfonatophenyl)Porphyrin

Daniel L. Akins,* Serdar Özçelik, Han-Ru Zhu, and Chu Guo

Center for Analysis of Structures and Interfaces (CASI), Department of Chemistry, The City College of The City University of New York, New York, New York 10031

Received: April 4, 1996; In Final Form: June 7, 1996[⊗]

Fluorescence decay dynamics and structure of a *meso*-tetrakis(*p*-sulfonatophenyl)porphyrin, referred to herein as either H_2TSPP^{4-} or TSPP, which aggregates in highly acidic homogeneous solution, are discussed. The fluorescence lifetime of the aggregate is found to depend on whether electronic excitation is to the B (Soret) state or the Q state. This finding is interpreted as indicating that the aggregate's effective size differs in the two cases. Also, a discussion is provided of possible nonradiative pathways that might affect measured fluorescence lifetimes. Specific structural changes that occur within the porphyrin upon N-protonation and incorporation within the aggregate are also discussed. Additionally, vibrational frequencies are assigned to specific bonds of the porphinato macrocycle, and comparisons are made between bond lengths in the aggregate environment and those of the monomeric dianion.

I. Introduction

Intense research interest into the formation, structures, and excited state optical dynamics of artificially ordered molecular systems is fostered by the participation of molecular aggregates in the complex mechanisms and ultrafast elementary steps of biological events,[1] as well as by their potential application in photonics.[2] The primary mechanism through which molecular aggregate structures in both natural and artificial systems are created is self-assembly through intrinsic intermolecular interactions. Often such self-assembled molecular aggregates assume a structure that can be classified as being of J- or H-type, defined by the relative orientations of induced transition dipoles of the constituent molecules, either "head-to-tail" or "head-to-head", respectively.[3] Structural pictures such as those provided by J- and H-aggregates have provided a framework for theoretical analysis of structure and dynamics of aggregated systems.

Electronic excitation of molecular aggregates frequently results in emission dynamics that differ from that of isolated molecules because of the formation of Frenkel excitons.[4] These excitons are delocalized as a result of intermolecular coupling-induced rapid transfer of energy between molecules. Such energy delocalization occurs more rapidly, in general, than other molecular processes, including longitudinal relaxation and vibrationally induced dephasing. As a result of the sharing of excitation, excited aggregates possess properties that are unique to their structure. In particular, for J-aggregates, absorption bands are significantly narrowed,[5−8] and enhancements occur for such phenomena as radiative decay rates,[9−11] third-order nonlinear optical susceptibilities,[10] and vibrational Raman band intensities.[12,13]

Studies concerned with molecular aggregation, however, have focused on the cyanine dyes, especially the prototypical cyanine, 1,1′-diethyl-2,2′-cyanine, also referred to as pseudoisocyanine or PIC. More recently, interest has expanded to aggregates of synthetic porphyrins, principally owing to the well-documented spectral properties of the electronic ground and excited states of the monomers[14,15] and the successful correlation of vibrational Raman spectral bands of such monomers with structure by both empirical associations and theoretical vibrational mode analyses.[16,17]

For porphyrins, most studies of structure and dynamics of aggregates have dealt with systems containing only small numbers of interacting monomers. In particular, dimeric systems, which have been formed by self-assembly,[18,19] by chemical linkage through a metal bridge,[20−26] or by way of a covalent bond, have been the primary focus of most investigations.[27,28] For such systems, the spatial alignment of the porphinato macrocycles for the two interacting porphyrin moieties is often assessable through UV−vis absorption measurements. Also, molecular exciton theory,[3] in large measure, describes the effects of intermolecular coupling, although the similar dimensions of interplane distance and the size of the monomeric species invalidate the point dipole approximation.[29] As a result, any theoretical study of absorption spectra requires a more detailed model in which vibronic coupling,[30,31] $\pi-\pi^*$ interaction,[29] and phonon scattering are incorporated.[6−8]

Detailed structure of molecules incorporated into aggregates and the intermolecular alignment between individual molecules are not decipherable from electronic absorption spectra, owing to the inherent broadness of absorption bands. Resonance Raman spectroscopy, however, is potentially a sensitive tool to probe molecular structure and, in fact, has been utilized to study dimers, mainly of either the "sandwich-type" or extended conformations. Such structures are quite different from that of the J-aggregates, which have been characterized as having, for example, "deck-of-cards" or "brick work" intermolecular arrangements. Moreover, the large separation between the two porphyrin rings in typical sandwich dimers in, for example, μ-oxo and μ-nitrido axially bridged complexes (i.e., respectively, $(FeTPP)_2O$ and $(FeTPP)_2N$) results in weak intermolecular coupling that is not easily discerned through bandshifts in the Raman spectrum. However, Raman studies of polymeric porphyrin aggregates formed in Langmuir−Blodgett films have recently been reported.[32] These latter systems evidence strong features caused by dipolar coupling. However, quantitative description is limited because of imprecisely known intermolecular arrangements and environmental effects ascribed to coupling with lattice motions in such heterogeneous media.

We report here, however, fluorescence lifetime and resonance Raman studies of the aggregate formed from *meso*-tetrakis(*p*-sulfonatophenyl)porphyrin (hereinafter referred to as H_2TSPP^{4-}

[⊗] Abstract published in *Advance ACS Abstracts,* August 1, 1996.

S0022-3654(96)01013-1 CCC: $12.00

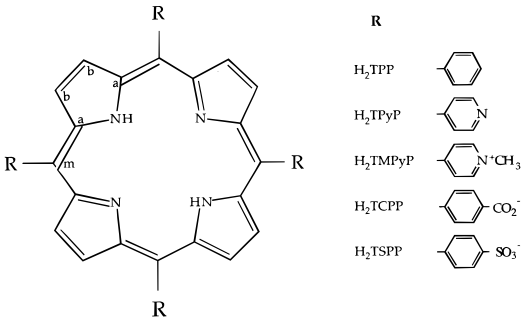

Figure 1. Structures of tetraarylporphines.

or TSPP; see Figure 1) in homogeneous solution, which appears to form the classic J-aggregate structure. H_2TSPP^{4-} forms aggregates in suitably acidic solution; typically, aggregation is aided by increasing the ionic strength through a moderate range.

The formation of aggregated, N-protonated TSPP ($H_4^{2+}TSPP^{4-}$) in homogeneous solution has been confirmed by this laboratory,[33] as well as by Ohno[34] and others,[35−38] and is indicated by the formation of a sharp J-type absorption band at 490 nm (B-band). In addition, a weak 705 nm absorption band (Q-band) is formed. Both of the aforementioned absorptions have been shown to be due to aggregated $H_4^{2+}TSPP^{4-}$ that is derived from monomeric dianionic $H_4^{2+}TSPP^{4-}$, as indicated by the diminution of the characteristic absorption for the monomer at 432 nm;[33] i.e., the aggregate is composed of N-protonated monomers. Furthermore, aggregation is indicated, based on comparison with our earlier observations with the cyanine dyes, by the enhancement of low-frequency vibrational Raman bands (at 241 and 317 cm^{-1}) when resonance excitation at ca. 490 nm is used to excite the Raman spectrum. For our studies all solutions have been aqueous and the temperature was ca. 22 °C.

More recently, we have shown through a conflation of electronic absorption, fluorescence and fluorescence excitation spectra, and vibrational Raman spectra of selected homogeneous solution phase tetraaryl-substituted porphyrins (free-base and protonated) that N-protonation induces structural changes that promote aggregation.[39] The tetraaryl porphyrins that we investigated were, in addition to H_2TSPP^{4-}, the following: tetraphenylporphyrin (H_2TPP), tetrapyridylporphyrin (H_2TPyP), tetrakis(*p*-4-methylpyridyl)porphyrin (H_2TMPyP^{4+}), and tetrakis(*p*-carboxyphenyl)porphyrin (H_2TCPP^{4-}); see Figure 1. Foremost, we found that aggregation is promoted when the porphyrin is converted upon protonation from a configuration in which the aryl moiety is twisted relative to the macrocycle plane to one in which it is nearly coplanar. It was also deduced that a basic requirement for aggregation is that the protonated species be zwitterionic.[39] We have gone further to suggest that the molecular subunits in an aggregated porphyrin are arranged in a cofacial fashion with a displacement between next nearest neighbors such that oppositely charged sites (e.g., positively charged central nitrogens and negatively charged sulfonato groups) are positioned close to one another, giving rise to J-aggregate type arrangements (specifically, spread "deck-of-cards" and "zigzag", both corresponding to head-to-tail alignments of the transition dipole moments).

In a present study, we have utilized fluorescence decay lifetime measurements (which provide information on exciton emission dynamics) and resonance Raman spectral data to gather additional insight into the structure of the N-protonated TSPP aggregate. From emission dynamics we deduce that an internal conversion competes with the exciton emission process ($S_2 \rightarrow S_0$), the internal conversion being between the S_2 (B) and the S_1 (Q) excited states of the porphyrin. We also ascertained that the fluorescence lifetime of the aggregate depends on whether

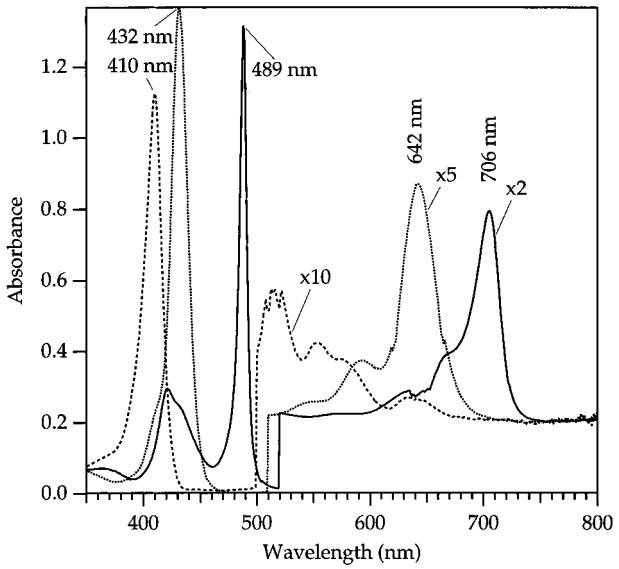

Figure 2. Absorption spectra of free-base (peak at 410 nm), monomeric dianion (peak at 432 nm), and aggregate (peak at 489 nm) TSPP. Concentration of TSPP in each case is 5×10^{-5} M in aqueous solution. For free-base, pH = 12; for monomeric dianion, pH = 4.5; for aggregate, pH = 1.6 and [KCl] is 0.1 M. Spectra above ca. 500 nm have been offset by +0.2 absorbance units and amplified by the indicated factor to enhance presentation. Structure on band near 500 nm for free-base is an artifact of the absorption spectrometer.

electronic excitation is to the B or the Q state. Our interpretation of this latter finding is that the aggregate's effective size differs in the two cases. We have also been able to deduce through Raman studies very specific structural changes that appear to occur within the porphyrin upon N-protonation and incorporation within the aggregate. We confirm some of our earlier determinations, such as the planar conformation of the intercalated monomers, but go further to assign vibrational frequencies to specific bonds of the porphinato macrocycle and compare bond lengths in the aggregate environment to those of the monomeric dianion.

II. Experimental Section

TSPP was purchased from Porphyrin Products, Inc., Utah, and used without further purification. Solutions were prepared using distilled and deionized water, pH values were adjusted by addition of 0.1 N NaOH or 0.1 N HCl, ionic strengths were varied through addition of KCl, and the concentration of the porphyrin in all solutions was maintained at ca. 5×10^{-5} M. Solutions were kept in the dark for 6−18 h prior to spectral measurements to allow species equilibration. Protonation and aggregation of the porphyrin were determined through the presence of characteristic absorption bands: 432 nm (monomeric dianion, $H_4^{2+}TSPP^{4-}$) and 490 and 705 nm (aggregated $H_4^{2+}TSPP^{4-}$). Typical absorption spectra for the monomeric dianion, the aggregate, and the free-base are shown in Figure 2, the presence of a particular species being determined by the pH at which the spectrum was attained.

A. Absorption and Fluorescence Apparatus. Absorption spectra were recorded using a Perkin-Elmer, Lambda 19, UV−vis−NIR spectrometer. Steady-state fluorescence, fluorescence excitation, and synchronously scanned luminescence spectra were acquired using a SPEX Fluorolog-τ2 spectrofluorometer. Principal components of the Fluorolog are the following: a 450 W xenon incandescent lamp coupled to both a single grating excitation spectrometer and an emission spectrometer; a Pockels cell that modulates the excitation light from 0.5 to 300 MHz for lifetime studies; a T-box sampling module, including an automated, four-position sample changer; two Hamamatsu

Model R928-P photomultiplier tubes, one used as a reference detector and operated in the direct-current acquisition mode and the other operated in the photon-counting acquisition mode. Scanning of excitation, emission, or both simultaneously is under computer control (SPEX DM3000F software run on a 486 PC). All data were stored and analyzed using vendor software.

B. Fluorescence Lifetime Apparatus. Two types of fluorescence decay instruments were employed: a phase modulation fluorometer, using incandescent and CW laser excitation sources, and a streak-camera spectrometer system, using a synchronously pumped picosecond dye laser system or a picosecond laser diode for excitation.

The phase modulation approach utilizes the SPEX Fluorolog-τ2 spectrofluorometer. When configured for lifetime measurements, radiation from a CW xenon incandescent light source or laser is directed to a Pockels cell. We used front-face illumination and radiation of several different frequencies. For the incandescent lamp, radiation of an appropriate band-pass was chosen by the excitation spectrometer; for cw laser excitation we used both a Spectra Physics, Model 2000, argon ion laser (for 488 nm excitation) and a Coherent, Model 899, Ti:sapphire laser (for frequencies greater than 700 nm). The excitation band-pass was chosen by setting the slit width of the excitation spectrometer and typically was ca. 4 nm, resulting from a 1 mm entrance slit width. Approximately 8% of modulated excitation light from the Pockels cell was directed to the reference detector and the remainder to the sample. To measure the fluorescence lifetime of the porphyrins, a reference standard, e.g., glycogen, and the sample are required. The fluorescence lifetime determination is made through an analysis that utilizes the relative phase shift and relative demodulation of the sample compared to that of the reference standard.

The streak-camera system utilized is manufactured by Hamamatsu (Model C4780, with ancillary electronics) and allows the capturing of both the temporal profile and the resolved emission spectrum, in combination with a dispersive spectrometer. The time resolution that we attained with this system was ca. 20 ps.

C. Raman Apparatus. Raman spectra of the various samples were excited at wavelengths that overlapped appropriate absorption bands. For the free-base and the monomeric dianion species, a Coherent tunable dye laser, Model CR-599, with an appropriate laser dye, was pumped by a CW 20 W, Coherent, Antares, argon ion laser. However, much less pump power (ca. 4 W) was used, and a three-plate birefringent filter produced radiation of ca. 1/4 Å bandwidth. The resonance Raman spectrum of the aggregated species was excited using the 488 nm excitation of the Antares. Raman spectra were recorded using a SPEX 1877, 0.6 m triple-spectrometer coupled to a charge-coupled-device (CCD) detector (Spectrum-1) cooled to 140 K with liquid nitrogen. Reported Raman spectra, in general, correspond to 1 scan with a 0.2 s (for aggregate) and 30 s (for N-protonated dianion monomer) integration period per scan. All Raman spectra reported here have been refined by background subtraction, by exporting files to analysis software (Igor) from Wavematrics (Lake Oswego, Oregon), and have a resolution of ca. ± 2 cm^{-1}.

III. Results and Discussions

A. Fluorescence and Decay Kinetics of the TSPP Aggregate. Fluorescence spectra of TSPP were obtained from solutions containing the free-base, the protonated dianionic monomer, or the aggregated dianion, achieved by adjusting the concentration and pH of the solution. Figure 3 shows fluorescence spectra resulting from excitation at the B-band absorption of the various species, specifically, 412, 432, and 488 nm for free-base, the dianion monomer, and the aggregate, respectively. We, moreover, established that the fluorescence spectrum for a particular species was the same whether excitation was in a B-band or a Q-band absorption. As specific examples, excitation at 642 nm for a solution containing the TSPP monomeric dianion results in a fluorescence that matches that found when 432 nm excitation is used, and excitation at 705 nm for a solution containing principally the aggregated TSPP dianion results in fluorescence that matched that found when 488 nm excitation was used.

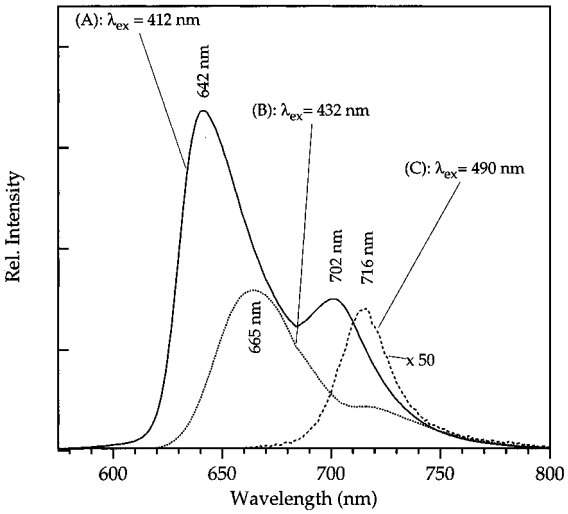

Figure 3. Fluorescence spectra of free-base (A), monomeric dianion (B), and aggregate (C) TSPP; solutions same as in Figure 4. Respective excitation wavelengths are indicated. Concentration of TSPP in each case is 5×10^{-5} M in aqueous solution. For free-base, pH = 12; for monomeric dianion, pH = 4.5; for aggregate, pH = 1.6 and [KCl] is 0.1 M. Annotation $\times 50$ indicates the amplification factor used.

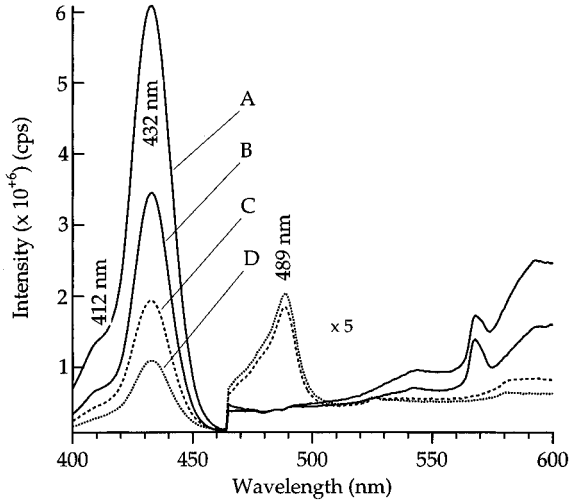

Figure 4. Excitation spectra as a function of pH. Emission detected at 665 nm (monomeric dianion) and 712 nm (aggregated dianion), where the concentration of TSPP in each case is 5×10^{-5} M in aqueous solution and no KCl was present, resulting in lower aggregate concentration than in Figure 3: (A) pH = 3, emission at 665 nm; (B) pH = 1.5, emission at 665 nm; (C) pH = 3.0, emission at 712 nm; (D) pH = 1.5, emission at 712 nm. Intensities (counts per second) for wavelengths greater than ca. 460 nm have been multiplied by a factor of 5.

We further ascertained that the excitation spectrum of the emission from a particular species matched the absorption spectrum of that species.[39]

Additionally, we have conducted studies that suggests that the ground-state aggregate absorbs more as pH is lowered. For example Figure 4 shows the influence of pH on the excitation spectra of the emission band at 665 nm, due to dianion

TABLE 1: Fluorescence Lifetime Measurements Using the Phase-Modulation and Streak-Camera Systems

	λ_{ex} (nm)	λ_{em} (nm)	τ_{fl} (ns)	χ^2
Phase Modulation				
free-base	414	658	9.5 (88%), 1.9 (12%)	0.93
	414	702	9.3 (87%), 4.3 (13%)	1.39
dianion monomer	432	675	3.9 (100%)	1.14
	642	675	3.5 (100%)	1.49
aggregate	488	720	0.295 (92%), 9.0 (8%)	1.5
	706	728	0.082 (83%), 1.7 (17%)	1.06
Streak Camera				
free-base	635	660−800	7.1 (100%)	0.95
dianion monomer	635	656−705	3.2 (100)%	1.14
	635	702−808	0.262 (56%), 3.4 (44%)	1.22
aggregate[c]	635	650−800	0.294 (46%), 3.4 (56%)	1.16
aggregate[d]	635	700−820	0.297 (56%), 3.5 (44%)	1.06
aggregate[e]	635	650−700	3.1 (100%)	1.16
Photon Counting[a]				
free-base	630	645	9.26 (100%)	*b*
dianion monomer	630	680	3.87 (100%)	*b*
aggregate	713	730	0.05 (94.8%), 0.29 (5%), 2.08 (0.2%)	*b*

[a] Values measured by Maiti *et al.* See ref 37. [b] Value not provided. [c] Two-week old sample. [d] Fresh sample. [e] Same sample as in *d*.

monomers, and the emission band at 715 nm, due to the aggregated dianion.

As a result of our findings, we conclude that emission occurs from the lowest excited electronic singlet state (S_1) associated with the Q-band, despite the fact that excitation might be to the S_2 state, the higher excited state associated with the B-band. In contrast to the observation of Maiti *et al.*,[37] we found no shifts of the 715 nm emission of the aggregate as a function of excitation wavelength, suggesting that only one type of aggregate exists for our samples. The emission at 715 nm, however, was substantially weaker than that from the other emitting species (see Figure 3). We interpret this observation in terms of radiative quenching pathways that may become operative upon aggregate formation (*vide infra*).

Fluorescence decay rates for emission at fluorescence maxima and excitation at absorption maxima for free-base, protonated, and aggregate TSPP were measured for B and Q state transitions. The results of fluorescence lifetime measurements in the author's laboratory using both the phase-modulation and streak-camera systems are shown in Table 1. Also included in the table are lifetimes determined through use of a single-photon counting technique.[37]

Our phase-modulation results indicate that the lifetime of the free-base is ca. 9.4 ns and that of the monomeric dianion ca. 3.5 ns, independent of whether B-band or Q-band excitation was used. For the aggregate, we measured a fluorescence lifetime of ca. 290 ps when B-band excitation at 488 nm was used but a lifetime of ca. 82 ps when Q-band excitation at ca. 706 nm was used.

The lifetimes of the free-base and the monomeric dianion that we found are in excellent agreement with photon-counting measured values reported in the literature.[37] The phase-modulation measured lifetime of the aggregate (290 ps), when we used 488 nm excitation, agrees with one component of the biexponential photon-counting decay found when 713 nm excitation was used.[79] However, the 290 ps relaxation is a minor component (5%) found in the latter study. The major component has an average relaxation time of 68 ps, while the shortest component is 50 ps (94.8%) and another minor component (0.2%) has a relaxation time of ca. 2 ns. For our Q-band excitation study, as indicated above, the major component has a relaxation time of 82 ps (83%); the second component has a relaxation time of ca. 1.8 ns (17%).

The fluorescence lifetime measurements shown in Table 1 accomplished with a streak camera are consistent with those found using our phase-modulation instrumentation. Any difference between the two can be explained as due to the difference in detection frequency band-pass.

Our speculation of the excitation wavelength dependence of fluorescence lifetime is that B-band excitation and Q-band excitation result in different coherence lengths for the Q state of the aggregate from which emission occurs. The indirect B-band excitation of the aggregate requires internal conversion (IC) between the S_2 and S_1 aggregate manifolds, which implicitly indicates that vibronic states are activated, which are known to cause localization of excitonic energy, resulting in decreased coherence length. The different coherence lengths (i.e., different numbers of molecules that are cooperatively coupled) translate into different radiative lifetimes, since molecular exciton theory indicates that radiative lifetime is inversely related to the number of molecules in the aggregate.[8−11] As a result, the radiative lifetime resulting from the indirect excitation into the Q state would be longer (the 290 ps measurement) than that associated with the direct Q state excitation.

We might note that an ultrafast fluorescence decay ($\tau_f < 10$ ps) is observed for sandwich complexes of lanthanide porphyrins,[26a] which has been attributed to the existence of nonradiative pathways that involve charge-transfer and/or triplet states of lower energy than the emitting $^1Q(\pi,\pi^*)$ state and, also, that molecular orbital theory has been successful in determining selection rules and character of such states. Since adjacent molecules in the aggregate experience interactions analogous to that of molecules in aligned sandwich complexes, it would seem appropriate to attempt to understand interactions between aggregate states, the wavelengths for excitation of such states (i.e., their relative locations), and their possible relaxation pathways by the formulation developed for sandwich porphyrins. The appropriate MO approach, in general, would be expected to involve more than just a molecular exciton model for the coupling between states of similar manifolds, such as B (Soret) and Q states for adjacent molecules, since the structure that we have envisaged for the aggregate is one in which the monomeric dianions are cofacially stacked—but translated along the axis defined by opposite *meso* carbons such that the negatively charged sulfonato group of the porphyrin moiety is positioned over the positively charged macrocycle moiety—suggesting strong Coulomb interaction as well as $\pi-\pi$ interactions between the π-electronic systems of the macrocycle and the phenyl substituent. A suitable formulation would appear to be the molecular orbital/configuration interaction model that has been used to interpret the presence of so-called "extra" Q-type absorption bands that are observed in absorption spectra of lanthanide porphyrin sandwich complexes.[26a,f,g] This formulation considers a cofacial porphyrin complex with strong electronic interaction between the two neighboring subunits, with molecular orbitals delocalized over the entire sandwich complex (i.e., the supermolecule approach). With this approach, and expressing the MOs of the sandwich complexes in terms of the four-orbital model (specifically, $a_{1u}(\pi)$ and $a_{2u}(\pi)$ HOMOs and $e_g(\pi^*)$ LUMOs) that describes the electronic states of the porphyrin monomer,[40] four dipole-allowed as well as four dipole-forbidden excited state configurations are obtained by one-electron promotion among the orbitals of the dimeric system. As a result of this supermolecule MO model, the singlet electronic states derived include the allowed B^+ and Q^+ exciton states formed by in-phase combinations of locally excited, adjacent monomers, which correspond to the Soret and Q(0,0) absorption bands, respectively, and two allowed charge resonance states (CR_1^+ and CR_2^+) that are formed by in-phase combination of the charge-transfer transitions (CT) between monomers, e.g., from the a_{1u} HOMO of one monomer to the e_g

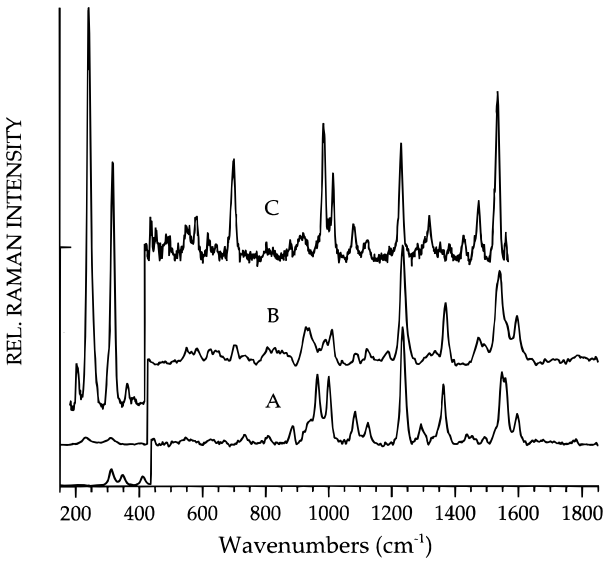

Figure 5. Resonance Raman spectrum of TSPP, where the solution is the same as in Figure 3 and spectra for wavenumbers greater than 400 nm have been amplified by a factor of 5 and offset to aid in visualization: (A) free-base, $\lambda_{ex} = 416$ nm, offset of 10K counts; (B) protonated dianion, $\lambda_{ex} = 432$ nm, offset of 20K counts; (C) aggregated dianion, $\lambda_{ex} = 488$ nm, offset of 35K counts.

LUMO of the other. These latter states have been shown to contribute to the so-called Q″ absorption that is often located between the B and Q absorption bands of sandwich complexes.[26e]

In addition to the states above, for sandwich complexes, the MO model indicates that two dipole-forbidden exciton states B^- and Q^-, formed by out-of-phase linear combination of the monomer specific B and Q excited states, are mixed with two dipole-forbidden charge resonance states CR_1^- and CR_2^-, giving rise to four dipole-forbidden singlet states. Of these latter states, the lowest energy one has been associated with a red-region absorption of the sandwich complexes and has been labeled as the Q′ band.[26e]

Returning to a consideration of the TSPP aggregate, we note that the aggregate's absorption spectrum (see Figure 2) does not indicate the presence of either Q″ or Q′ bands. Hence, CT states do not appear to play an important role in determining dipole-allowed radiative transitions, which supports the idea that measured lifetimes reflect exciton coupling and its influence on coherence length. However, excitonic states near the bottom of the Q^- state, even though not dipole-allowed for transitions to the ground state (specifically, the Q subbands), with their decreased separation from the S_0 state, have been suggested as states that lead to a decrease of the fluorescence lifetime of porphyrin sandwich complexes.[24]

The lifetime of the Q state that we have measured (82 ps, 83%, $\chi^2 = 1.06$),[78] using the phase modulation technique (with CW Ti:sapphire excitation at 706 nm), and the minimum lifetime of the Q state reported by Maiti *et al.*[37] (50 ps, 95%, $\chi^2 = ?$), using the single-photon counting technique, are sufficiently close, given the differences in experimental conditions, to confirm the shorter lifetime of the Q state excited aggregate in relation to that of the B state excited aggregate.

Finally, it might be pointed out that in addition to the Q subband pathway to shortening the fluorescence lifetime, as mentioned above, there is another mechanism for quenching fluorescence. This mechanism involves intermolecular phonon modes that incorporate motion in the aggregate formation direction.[41] Such a nonradiative pathway seems particularly apropos given the formation of low-frequency intermolecular vibrations (resonance Raman bands at 241 and 317 cm^{-1}; see Figure 5C) upon resonant excitation into the B-band aggregate absorption band, which in resonance Raman studies of cyanine dyes has been interpreted as signaling the activation of intermolecular phonon modes.[42]

Mechanisms such as those mentioned above may indeed explain the shortened lifetime and weak fluorescence one observes from the aggregate.

TABLE 2: Assignment of the Resonance Raman Bands of Aggregated, Protonated Dianion, and Free-Base TSPP[a]

aggregated	protonated	free-Base	assignments*
205 (1.60)			
241 (16.8)	233 (0.31)		γ_s(por) core ruffling?
317 (10.2)	310 (0.30)		γ_s(por) core doming?
362 (0.88)		348 (0.35)	ν(N...N)
435 (vw)	405 (0.06)	412 (0.38)	?
549 (vw)	549 (0.13)	548 (0.06)	?
583 (0.36)	582 (0.12)		?
618 (vw)	625 (0.12)	629 (0.04)	phenyl
700 (0.86)	701 (0.15)		?
728 (vw)	734 (0.06)	734 (0.08)	?
808 (vw)	805 (0.14)	805 (0.07)	B_{1g}, δ_s(pyr)
882 (vw)		887 (0.16)	A_{1g}, δ_s(pyr)? phenyl?
920 (0.23)	929 (0.30)	920 (vw)	
985 (1.16)	990 (0.20)	964 (0.60)	A_{1g} (pyr ring breathing)
1014 (0.74)	1010 (0.28)		A_{1g} (pyrrolenine ring breathing)
1082 (0.28)	1084 (0.08)	1084 (0.28)	A_{1g}, $\delta_s(C_b-H)$
1124 (0.15)	1122 (0.12)	1125 (0.19)	A_{1g}, $\nu(C_a-N)$
1195 (sh)	1189 (0.10)	1197 (vw)	B_{1g}, $\nu_a(C_a-C_b)$
1230 (1.00)	1235 (1.00)	1234 (1.00)	$\nu(C_m-\Phi)$
1284 (0.13)	1284 (sh)		B_{1g}, $\nu_s(C_a-N)$, $[\nu(C_a-N)\ \{NH\}]^a$
1318 (0.38)	1320 (0.08)		B_{1g}, $\nu_{as}(C_a-N)$
1354 (0.16)	1338 (0.10)		A_{1g}, $\nu_s(C_a-C_b) + \nu_s(C_a-N)$
1384 (0.15)	1370 (0.15)	1363 (0.51)	A_{1g}, $\nu_s(C_a-N) + \nu_s(C_a-C_b)$
1428 (0.21)	?	1293 (0.17)	A_{1g}, $\nu_s(C_a-C_b)$
1476 (0.50)	1474 (0.22)	1493 (0.06)	B_{1g}, $\nu(C_b-C_b)$, $[A_{1g}, \nu(C_b-C_b)\ \{NH\}]^a$
1534 (1.44)	1541 (0.78)	1548 (0.62)	A_{1g}, $\nu(C_b-C_b)$, $[A_{1g}, \nu(C_b-C_b)\ \{N\}]^a$
1561 (0.24)	1566 (sh)	1437 (0.09)	B_{1g}, $\nu_{as}(C_a-C_m)$
		1559 (0.59)	?
1594 (0.26)	1596 (0.40)	1597 (0.26)	phenyl

[a] Free-base TSPP. [b] Symbol * is used to indicate that bonds are specified by the atom labeling indicated in Figure 1. {NH} and {N} refer to the pyrrole and the pyrrolenine rings, respectively. ν represents bond stretching, δ represents bond bending, and γ represents ring deformation. Subscripts s and as refer to the symmetric and asymmetric vibrations with respect to the pyrrole 2-fold axis for $\nu(C_b-H)$, $\delta(C_b-H)$, $\nu(C_a-N)$, or the methine 2-fold axes for $\nu(C_a-C_b)$. pyr and por represent, respectively, the pyrrole ring and the porphinato macrocycle and Φ the phenyl group.

B. Resonance Raman Spectra and Band Assignments of Aggregated TSPP. Raman spectra of free-base, monomeric dianion, and aggregated dianion TSPP were resonantly excited at the appropriate B-band absorption wavelength and are shown in Figure 5. A compendium of correlated bands is shown in Table 2. Cursory analysis of the resonance Raman (RR) spectra of the monomeric dianion and aggregated dianion shown in Figure 5 reveals obvious associations between bands of the two species, which do not accommodate bands of the free-base porphyrin.

Closer scrutiny, however, reveals that subtle differences, as might be expected, exist between the correlated bands of the aggregate and the dianionic monomer, which suggests that intermolecular interactions between molecules of the aggregate are expressed through such differences. The most dramatic difference in spectra is found in the low-frequency region, where two bands of dianionic TSPP monomer at 233 and 310 cm^{-1} correlate with two dramatically enhanced aggregate bands (by a factor of more than 30!) at 241 and 317 cm^{-1}. These latter bands, moreover, are accompanied by two satellite bands at 205 and 362 cm^{-1}.

Bands at low frequency, even for porphyrin monomers, have not been assigned as confidently as those in the high-frequency region, associated with in-plane skeletal vibrations and are the features that would be most influenced by the intermolecular coupling that promotes aggregation.

In the literature, the low-frequency Raman bands of porphyrins have been suggested as deriving from out-of-plane modes, including bending of the C−Φ bond (Φ representing phenyl) and deformation of the core of the porphinato macrocycle due to pyrrole-ring tilt and swivel.[15,43−45] Also, in the case of lanthanide sandwich dimer porphyrins, low-frequency Raman bands have been postulated to reflex the extent of intramolecular $\pi-\pi$ interaction and to be associated with the intradimer vibration that modulates the separation between the two porphyrin moieties or due to symmetrical linear combinations of out-of-plane deformations of the adjacent porphinato macrocycles.[24]

Hence, the presence of bands at 233 and 310 cm^{-1} for protonated TSPP monomer is likely attributable to out-of-plane doming and ruffling of the central core defined by the four pyrrole nitrogen atoms in which the nitrogen atoms are alternately positioned up or down with respect to the average plane of the central core of the macrocycle. This latter assignment is in agreement with semiempirical calculations that we have performed that indicate that protonation of free-base porphyrins leads to out-of-plane arrangements of the (resultant) four N−H bonds of the macrocycle.

In the high-frequency regime of the spectra shown in Figure 5, attributable to skeletal motion of the porphinato macrocycle, relative spectral differences are also apparent upon detailed examination.

To make an assessment of the magnitude and direction of "changes", i.e., to associate particular bands of the various species with one another, we have taken the view that semiempirical AM1 calculations for porphyrin free-base and monomeric dianion band positions provide references for assigning frequencies to particular molecular vibrations of the two species.[45,46] As a result of such assignments, bands of the aggregate that correlate because of their positions allow inferences to be made concerning structural distortions and intermolecular interaction between adjacent porphinato macrocycles. Table 2 reflects assignments made through such a scheme and by comparison to the literature, which has typically used resonance Raman spectroscopy to access structure for porphyrin complexes with either stacked "face-to-face" or "edge-to-edge" extended architectures.

Structure and intermolecular interaction information for stacked complexes have resulted from analysis of the resonance Raman spectrum of $(FeTPP)_2O$ by Adar *et al.*,[20] based on resonance Raman selection rules for dimers, who anticipated "extra" vibrational bands due to splitting caused by intradimeric exciton coupling. The absence of such bands in $(FeTPP)_2O$ [refs 21 and 22] and $(FeTPP)_2N$ [refs 23 and 24] has been interpreted as indicating insubstantial orbital overlap between the two porphyrin moieties as a result of their large separation: 4.6 Å for μ-$(FeTPP)_2O$ and 4.2 Å for μ-$(FeTPP)_2N$ dimers.

The effect of inter-ring separation has been substantiated by the observation of bandshifts in Raman spectra of lanthanide porphyrin sandwich dimers and triple-decker complexes (e.g., (OEP)Ln(OEP)Ln(OEP)Ln, where Ln includes La^{III}, Ce^{III}, and Eu^{III}) for which the distance between the macrocycle planes (defined by the four nitrogen atoms) ranged from 2.6 to 3.5 Å, depending on the size of the lanthanide ion.[25] Additional evidence in support of the importance of orbital overlap comes from the finding that the spectral shifts for these sandwich complexes are strongly affected by steric effects of substituents located at *meso* carbon atoms (e.g., see C_m in Figure 1) rather than by the electron donating/withdrawing character of substituents attached peripherally to the porphyrin rings.[24d]

Also, the requirement of substantial $\pi-\pi$ interaction is suggested from Raman studies involving covalently linked porphyrins dimers.[27] Again, the bandshifts, relative to monomer band positions, are observed only for dimers in which the molecular planes of the two porphyrin moieties have a parallel alignment.

Thus, from the Raman probing of porphyrin dimers of different arrangements one can conclude that dimeric complexes are primarily perturbed through $\pi-\pi$ interaction of two adjacent moieties, provided the nitrogen planes of the porphyrin macrocycles are aligned cofacially and their inter-ring separation is small.

As a result of the above, we anticipate that Raman bandshifts for aggregated TSPP (relative to those of protonated TSPP) can be attributed to intermolecular interactions. Consequently, analysis of Raman bandshifts should provide information concerning structural distortion induced by the aggregate environment. Band assignments that incorporate issues as addressed here are provided in Table 2. An additional concession to simplify Table 2 is that the Raman band assignment identifies only the major participating vibrational motion, despite the fact that internal coordinates for the porphyrin normal modes are undoubtedly significantly mixed. Such a simplification, however, appears reasonable based on our recent AM1 semiempirical calculations on free-base porphine (PH_2) and tetrafluoroporphine ($TFPH_2$),[46,47] which indicate a monotonic correlation of the Raman bandshifts with change in skeletal bond lengths of the porphinato macrocycle.

As a result of our empirical assignments, we have deduced, for protonated TSPP incorporated within an aggregate, that the 1534 cm^{-1} band is due to stretching while the correlated band for the unincorporated monomeric dianion occurs at 1541 cm^{-1} and for the free-base at 1548 cm^{-1}. Thus, incorporation of the dianion into the aggregate appears to result in a downshift of the in-plane symmetric stretch of C_b-C_b, where the atom designation, here as well as below, utilizes the labeling shown in Figure 1. Similar comparisons for other bands for unincorporated vs incorporated dianion suggest the following: the Raman band attributable to the C_a-C_b in-plane vibration upshifts from 1338 to 1354 cm^{-1}; skeletal vibrations represented by the C_a-C_m and C_a-N bonds are alternately upshifted and downshifted.

Distortions of structure such as suggested by the direction of bandshifts are to be expected when an electron is partially withdrawn from the a_{2u} orbital of the porphinato macrocycle, as would be expected to occur for the aggregate structure we have advanced that anticipates the strong intermolecular Coulombic interaction between oppositely charged sites of two adjacent protonated TSPP moieties. Also, such interpretations as above are congruent with our AM1 semiempirical calculation that indicates that the C_b-C_b bonds of PH_2 and $TFPH_2$ are lengthened upon protonation of the respective free-base.[46,47]

IV. Conclusion

In this article, the author focuses on the structure and fluorescence decay dynamics of aggregated *meso*-tetrakis(*p*-sulfonatophenyl)porphyrin (TSPP). Structural changes, such as twisting of the aryl moiety to a nearly coplanar alignment with the macrocycle structure, have been deduced from Raman scattering measurements. Assignments of vibrational bands have been made that are facilitated by a comparison with the band positions of the free-base and the monomeric dianion, as well as with the aid of AM1 calculations.

Fluorescence spectra and fluorescence lifetime measurements following B- and Q-band excitation of free-base, monomeric dianion, and aggregated TSPP have been conducted and interpreted as indicating that internal conversion and nonradiative pathways play important roles in exciton behavior in the aggregated system. One of the key findings regarding the optical dynamics of aggregated TSPP is that the fluorescence lifetime of the Q state of the aggregate can have one of two values, depending on whether the excitation is initially to the B state or to the Q state.

Acknowledgment. Support for this research by the National Science Foundation (NSF) under Grant HRD-9353488 and contributions by W. Cieslik (of Hamamatsu Photonics) are gratefully acknowledged.

References and Notes

(1) (a) Okamura, M. Y.; Feher, G. In *Photosynthesis: Energy Conversion by Plants and Bacteria*; Academic Press: New York, 1982; Vol, 1, pp 195−272. (b) Hofman B. M.; Ibers, J. A. *Acc. Chem. Res*. **1983**, *16*, 15−21. (c) Diesenhofer, J.; Epp, O.; Miki, K.; Huber, R.; Michel, H. *J. Mol. Biol*. **1984**, *180*, 385−398. (d) Diesenhofer, J.; Epp, O.; Miki, K.; Huber, R.; Michel, H. *Nature (London)* **1985**, *318*, 618−624. (e) Chang, C.-K.; Tiede, D.; Tang, J.; Smith, U.; Shiffer, M. *FEBS. Lett.* **1986**, *205*, 82−86. (f) Allen, J. P.; Feher, G.; Yeates, T. O.; Komiya, H.; Rees, D. C. *Proc. Natl. Acad. Sci. U.S.A.* **1987**, *84*, 6730−5734.

(2) (a) Martinsen, J.; Stanton, J. L.; Greene, R. L.; Tanaka, J.; Hoffman, B. M.; Ibers, J. A. *J. Am. Chem. Soc*. **1985**, *107*, 6915−6920. (b) Ogawa, M. Y.; Martinsen, J.; Palmer, S. M.; Stanton, J. L.; Tanaka, J.; Greene, R. L.; Hoffman, B. M. Ibers, J. A. *J. Am. Chem. Soc*. **1987**, *109*, 1115−1121. (c) Turek, P.; Petit, P.; Andre, J.-J.; Simon, J.; Even, R,; Boudjema, B.; Guillaud, G.; Maitrot, M. *J. Am Chem. Soc*. **1987**, *109*, 5119−5122. (d) Nohr, R. S.; Kuznezof, P. M.; Wynne, K. J.; Kenney, M. E.; Seibenman, P. G. *J. Am. Chem. Soc*. **1981**, *103*, 4371−4377. (e) Diel, B. N.; Inabe, T.; Lyding, J. W.; Schoch, K. F., Jr.; Kannewurf, C. R.; Marks, T. J. *J. Am. Chem. Soc*. **1983**, *105*, 1551−1567. (f) Pietro, W. J.; Marks, T. J.; Ratner, M. A. *J. Am. Chem. Soc*. **1985**, *107*, 5387−5391. (g) Diel, B. N.; Inabe, T.; Tagg, N. K.; Lyding, J. W.; Schneider, O.; Hanak, M.; Kennewurf, C. R.; Marks, T. J.; Schwartz, L. H. *J. Am. Chem. Soc*. **1984**, *106*, 3207−3214. (h) Collman, J. P.; McDevit, J. T.; Leidner, C. R.; Yee, G. T.; Torrance, J. B.; Little, W. A. *J. Am. Chem. Soc*. **1987**, *109*, 4606−4614. (i) Hale, P. D.; Pietro, W. J.; Ratner, M. A.; Ellis, D. E.; Marks, T. J. *J. Am. Chem. Soc*. **1985**, *107*, 5943−5947.

(3) Kasha, M. *Radiat. Res*. **1963**, *20*, 55.

(4) Frenkel, J. I. *Phys. Rev.* **1931**, *37*, 17, 1276.

(5) Scherer, P. O. J.; Fischer, S. F. *Chem. Phys*. **1984**, *86*, 269.

(6) Knapp, E. W.; Scherer, P. O. J.; Fischer, S. F. *Chem. Phys. Lett*. **1984,** *111*, 481.

(7) Knapp, E. W. *Chem. Phys*. **1984**, *85*, 73.

(8) Spano, F. C.; Mukamel, S. *J. Chem. Phys*. **1989,** *91*, 683.

(9) Grad, J.; Hernandez, G.; Mukamel, S. *Phys. Rev. A*. **1988**, *37*, 3835.

(10) Spano, F. C.; Kuklinski, J. R.; Mukamel, S. *Phys. Rev. Lett.* **1990**, *65*, 211.

(11) Spano, F. C.; Mukamel, S. *Phys. Rev*. **1989**, *40A*, 5783.

(12) Akins, D. L. *J. Phys. Chem*. **1986**, *90*, 1530.

(13) Akins, D. L.; Lombardi, J. R. *Chem. Phys. Lett*. **1987**, *136*, 495.

(14) Smith, K. M., Ed. *Porphyrins and Metalloporphyrins*; Elsevier: New York, 1975.

(15) Gouterman, M. In *The Porphyrins*; Dolphin, D., Ed.; Academic Press: New York, 1979; Vol. 3, p 1.

(16) Kitagawa, T.; Ozaki, Y. *Struct. Bonding (Berlin)* **1987**, *64*, 1.

(17) Spiro, T. G.; Li, X.-Y. In *Biological Applications* of *Raman Spectoscopy*; Spiro, T. G., Ed.; Wiley-Interscience: New York, 1988; Vol. 3, Chapter 1.

(18) (a) Fleischer, E. B.; Palmer, J. M.; Srivastava, T. S.; Chatterjee, A. *J. Am. Chem. Soc*. **1971**, *93*, 3162. (b) Pasternack, R. F.; Francesconi, L.; Raff, D.; Spiro, E. *Inorg. Chem*. **1971**, *12*, 2606. (c) Pasternack, R. F.; Huber, P. R.; Boyd, P.; Engasser, G.; Francesconi, L.; Gibbs, E.; Fasella, P.; Venturo, G. C.; deC. Hinds, L. *J. Am. Chem. Soc*. **1972**, *94*, 4511. (d) Krishnamurthy, M.; Sutter, J. R.; Hambright, P. *J. Chem. Soc., Chem. Commun*. **1975**, *13*.

(19) (a) Kano, K.; Miyaki, T.; Uomoto, K.; Sato, T.; Ogawa, T. Hashimoto, S. *Chem. Lett*. **1983**, 1867. (b) Chandrashekar, T. K.; Van Willigen, H. *Chem. Phys. Lett*. **1984**, *106*, 237. (c) Ojadi, E.; Selzer, R.; Linschitz, H. *J. Am. Chem. Soc*. **1985**, *107*, 7783. (d) Van Willigen, H. Da, U.; Ojada, E.; Linschitz, H. *J. Am. Chem. Soc*. **1985**, *107*, 7784. (e) Hofstra, U.; Koehorst, R. B. M.; Schaafsma, T. J. *Chem. Phys. Lett*. **1986**, *130*, 555. (f) Geiger, D. K.; Kelly, C. A. *Inorg. Chim. Acta* **1988**, *154*, 137. (g) Vergeldt, F. J.; Koehrst, R. B. M.; Schaafsma, T. J.; Lambry, J.-C.; Martin, J.-L.; Johnson, D. G.; Wasielewski, M. R. *Chem. Phys. Lett*. **1991**, *182*, 107. (h) Hugerat, M.; van der Est, A.; Ojadi, E.; Biczok, L.; Linschitz, H.; Levanon, H.; Stehlik, D. *J. Phys. Chem*. **1996**, *100*, 495.

(20) Adar, F.; Srivastava, T. S. *Proc. Natl. Acad. Sci. U.S.A.* **1975**, *72*, 4419.

(21) Burke, J. M.; Kincaid, J. R.; Spiro, T. G. *J. Am. Chem. Soc*. **1978**, *100*, 6077.

(22) (a) Schick, G. A.; Bocian, D. F. *J. Am. Chem. Soc*. **1980**, *102*, 7982. (b) Schick, G. A.; Bocian, D. F. *J. Am. Chem. Soc*. **1983**, *105*, 1830.

(23) Hofmann, J. A., Jr.; Bocian, D. F. *J. Phys. Chem*. **1984**, *88*, 1472.

(24) (a) Donohoe, R. J.; Duchowski, J. K.; Bocian, D. F. J. *Am. Chem. Soc*. **1988**, *110*, 6119. (b) Duchowski, J. K.; Bocian, D. F. *J. Am. Chem. Soc*. **1990**, *112*, 3312. (c) Duchowski, J. K.; Bocian, D. F. *Inorg. Chem.* ***1990***, *29*, 4158−4160. (d) Perng, J.-H.; Duchowski, J. K.; Bocian, D. F. *J. Phys. Chem*. **1990**, *94*, 6684. (e) Perng, J.-H.; Duchowski, J. K.; Bocian, D. F. *J. Phys. Chem*. **1991**, *95*, 1319. (f) Martin, P. C.; Arnold, J.; Bocian, D. F. *J. Phys. Chem.* **1993**, *97*, 1332.

(25) Duchowski, J. K.; Bocian, D. F *J. Am. Chem. Soc*. **1990,** *112*, 8807.

(26) (a) Yan, X.; Holten, D. *J. Phys. Chem*, **1988**, *92*, 409. (b) Bilsel, O.; Rodriguez, J.; Holten, D. *J. Phys. Chem.* **1990**, *90*, 3508. (c) Bilsel, O.; Rodriguez, J.; Girolami, G. A.; Milam, S. N.; Suslick, K. S. *J. Am. Chem. Soc.* **1990**, *112*, 4075. (d) Bilsel, O.; Buchler, J.; Hammerschmit, P.; Rodriguez, J.; Holten, D. *Chem. Phys. Lett*. **1991**, *182*, 415. (e) Bilsel, O.; Rodriguez, J.; Milam, S. N.; Gorlin, P. A.; Girolami, G. S.; Suslick, K. S.; Holten, D. *J. Am. Chem. Soc*. **1992**, *114*, 6528. (f) Bilsel, O.; Milam, S.; Girolami, G. S.; Suslick, K. *J. Phys. Chem.* **1993**, *97*, 7216. (g) Wittmer, L. L.; Holten, D. *J. Phys. Chem*. **1996**, *100*, 860.

(27) (a) Chang, C. K. *J. Heterocycl. Chem* **1977**, *14*, 1285. (b) Anderson, A. B.; Gordon, T. L.; Kenney, M. E. *J. Am. Chem. Soc.* **1985**, *107*, 192. (c) Kaizu, Y.; Maekawa, H.; Kobayashi, H. *J. Phys. Chem*. **1986**, *90*, 4234. (d) Maruyama, K.; Kobayashi, F.; Osuka, A. *Chem. Lett*. **1987**, 821. (e) Osuka, A.; Maruyama, K. *Chem. Lett*. **1987**, 825. (f) Osuka, A.; Maruyama, K.; Yamazaki, I.; Tamai, N. *J. Chem. Soc., Chem. Commun*. **1988,** 143. (g) Nagata, T.; Osuka, A.; Maruyama, K. *J. Am. Chem. Soc*. **1990,** *112*, 3054. (h) Hunter, C. A.; Meah, N.; Sanders, J. K. M. *J. Am. Chem. Soc*. **1990,** *112*, 5773. (i) Kessel, D.; Byrne, C. J.; Ward, D. *Photochem. Photobiol*. **1991**, *53*, 469. (j) Zaleska, J. M.; Chang, C. K.; Nocera, D. G. *J. Phys. Chem*. **1993**, *97*, 13206.

(28) (a) Greiner, S. P.; Winzenburg, J.; Von Maltzan, B.; Winscom, C. J.; Mobius, K. *Chem. Phys. Lett.* **1989** *155*, 93. (b) Gosztola, D.; Wasielewski, M. R. *J. Phys. Chem*. **1993**, *97*, 9699.

(29) Hunter, C. A.; Sanders, J. K. M.; Stone, A. *Chem. Phys. Lett*. **1989**, *133*, 395.

(30) Fulton, R. L.; Gouterman, M. *J. Chem. Phys*. **1961**, *35*, 1059; **1964**, *41*, 2280.

(31) (a) Piepho, S. B.; Krausz, E. R.; Wschatz, P. V. *J. Am. Chem. Soc*. **1978**, *100*, 2996. (b) Piepho, S. B. *J. Am. Chem. Soc*. **1988**, *110*, 369.

(32) (a) Schick, G. A.; Schreiman, I. C.; Wagner, R. W.; Lindsey, J. S.; Bocian, D. F. *J. Am. Chem. Soc*. **1989**, *111*, 1344. (b) Schick, G. A.; O'Grady, M. R.; Tiwari, R. K. *J. Phys. Chem*. **1993**, *97*, 1339.

(33) Akins, D. L.; Zhu, H.-R.; Guo, C. *J. Phys. Chem*. **1994**, *98*, 3612.

(34) Ohno, O.; Kaizu, Y.; Kobayashi, H. *J. Chem. Phys*. **1993**, *99*, 4128.

(35) Ribo, J. M.; Crusats, J.; Farrera, J.-A.; Valero, M. L. *J. Chem. Soc., Chem. Commun*. **1994**, 681.

(36) Pasternack, R. F.; Schaefer, K. F.; Hambright, P. *Inorg. Chem*. **1994**, *33*, 2062.

(37) Maiti, N.; Ravikanth, M.; Mazumdar, S.; Periasamy, N. *J. Chem. Phys*. **1995**, *99*, 17159.

(38) Hutchison, M. T.; Schick, G. A. *Inorg. Chem.*, preprint.

(39) Akins, D. L.; Zhu, H.-R.; Guo, C. *J. Phys. Chem*. **1996**, *100*, 5420.

(40) Gouterman, M. *J. Chem. Phys*. **1959**, *30*, 1139.

(41) (a) Fidder, H.; Knoster, J.; Wiersma, D. A. *Chem. Phys. Lett*. **1990**, *171*, 529. (b) Fidder, H.; Terpstra, J.; Wiersma, D. A. *J. Chem. Phys*. **1991**, *94*, 6895.

(42) (a) Akins, D. L.; Macklin, J. W.; Parker, L. A.; Zhu, H.-R. *Chem. Phys. Lett.* **1990**, *169*, 564. (b) Akins, D. L.; Zhuang, Y.-H.; Zhu, H.-R.; Liu, J.-Q. *J. Phys. Chem*. **1994**, *98*, 1068.

(43) (a) Kitagawa, T.; Abe, M.; Kyogoku, Y.; Ogoshi, H.; Watanabe, E.; Yoshida, Z. *J. Phys. Chem*. **1978**, *80*, 1181. (b) Kitagawa, T.; Abe, M.; Ogoshi, H. *J. Chem. Phys*. **1978**, *69*, 4516. (c) Ozaki, Y.; Iriyama, K.; Ogoshi, H.; Ochiai, T.; Kitagawa, T. *J. Phys. Chem*. **1986**, *90*, 6113.

(44) (a) Choi, S.; Spiro, T. G. *J. Am. Chem. Soc*. **1983,** *105*, 3683. (b) Li, X.-Y.; Czernuswicz, R. S.; Kincaid, J. R.; Spiro, T. G. *J. Am. Chem. Soc*. **1989**, *111*, 7012. (c) Czernuswicz, R. S.; Li, X.-Y.; Spiro, T. G. *J. Am. Chem. Soc*. **1989**, *111*, 7024. (d) Li, X.-Y.; Zgerski, M. Z. *J. Phys. Chem*. **1991**, *95*, 4268.

(45) Alden, R. G.; Crawford, B. A.; Doolen, R.; Ondrias, M. R.; Shelnutt. J. A. *J. Am. Chem. Soc*. **1989**, *111*, 2070.

(46) Ma, S.-Y.; Li, Z.-H.; Akins, D. L.; Zhu, H.-R.; Guo, C. Electronic Effect of meso-Substituents on the Structure of Porphinato Macrocycles upon Aggregation. To be submitted.

(47) Ma, S.-Y., Li, Z.-H.; He, J.-Y.; Akins, D. L.; Zhu, H.-R.; Guo, C. Protonation Induced Structural Changes in Porphine: Quantum Chemical and Resonance Raman Investigation. To be submitted.

JP961013V